PATTERN SPEED DOMAINS IN RINGED DISK GALAXIES FROM OBSERVATIONAL AND SIMULATIONAL DATABASES

G. BYRD
Department of Physics and Astronomy, University of Alabama, Tuscaloosa, Alabama 35487-0324

P. RAUTIAINEN AND H. SALO
Department of Astronomy, University of Oulu, Oulu, Finland

R. BUTA[1] AND D. A. CROCKER[1]
Department of Physics and Astronomy, University of Alabama, Tuscaloosa, Alabama 35487-0324

Received 1994 January 14; revised 1994 March 15

ABSTRACT

New test-particle simulations have been carried out to learn more about the secular evolution and morphology of the gaseous and stellar distributions in barred galaxies. We verify the previous results of M. P. Schwarz that gas clouds will tend to collect into ring-like patterns near major orbit resonances, owing to gravity torques. However, we improve on these results in several ways. Firstly, we use more gas clouds (10 000 vs 2000) than Schwarz and track individual clouds to determine when they collide, rather than using a collision box as did Schwarz. Secondly, besides Schwarz's isochrone rotation curve, we also use a flat rotation curve. Thirdly, we consider more bar pattern speeds and strengths than did Schwarz. Finally, unlike Schwarz and other simulators, we have a large database of images and color index maps of nearly 140 ringed galaxies that can be compared to the simulations to evaluate their significance. We confirm the two types of outer Lindblad resonance rings that Schwarz discovered, but find that their existence is not due so much to the initial density distribution of gas clouds as to pattern speed and the time interval since the bar potential was imposed. The simulations and the images lead us to suggest that we can divide barred galaxies according to the resonances which the bar pattern speed and rotation curve allow in the disk. We illustrate specific galaxies that we believe belong to fast, medium, and slow bar pattern speed "domains" and match them to particular simulation frames. We also discuss alternative hypotheses in which the pattern speed is such that all resonances are present but the gas has been depleted or was distributed differently in various galaxies to produce the three classification domains.

1. INTRODUCTION

Galaxy pattern speeds are one of the fundamental unknowns of galactic dynamics. As discussed by Kalnajs (1992), pattern speeds provide information on the equilibrium state of galaxy disks, halo contributions to this equilibrium, and the origin of spiral structure. For example, it has been recognized since the 1960's that resonances with the pattern speed of a spiral density wave can determine the structure and evolution of a galaxy's morphology, and that different resonances play different roles in this evolution. The Lindblad resonances, in particular, have been linked to limiting the propagation of spiral density waves across the disk. However, Kalnajs pointed out how, in the case of a high pattern speed where the corotation and outer Lindblad resonances (CR and OLR, respectively) are well within the visible disk, then the density wave pattern need not be spiral but could be a bar or an oval.

Although *direct* methods of estimating pattern speeds do exist, they are usually difficult to apply in practice. Methods tried so far involve application of the continuity equation to velocity and luminosity data of an SB0 galaxy (Tremaine & Weinberg 1985; Kent 1987; Kent & Glaudell 1989); the fitting of an "orbit model" to the two-dimensional velocity field of an inner ring of H II regions (Buta 1986b); analysis of net streaming motions in the disk (Canzian 1993); and detailed modeling of the gas flow in a fixed potential (Garcia-Burillo *et al.* 1993). Such analyses are time consuming and cannot be applied to all disk galaxies, and so as a consequence little is known about how pattern speed varies along the Hubble sequence or within a given Hubble type. It is also unclear whether the different features we may see in a given galaxy all have the same pattern speed (Sellwood & Sparke 1988).

Given the difficulty of direct measurement of pattern speeds, it is worth considering the use of more *indirect* methods. Kalnajs (1992) (see also Sellwood & Wilkinson 1993) discusses the use of the locations of "distinct features predicted by theory which are sensitive to the value of the pattern speed." In the case of so-called "grand-design" spiral galaxies, a variety of features has been used in the past, such

[1]Visiting Astronomer, Cerro Tololo Inter-American Observatory, National Optical Astronomy Observatories, operated by the Association of Universities for Research in Astronomy, Inc. (AURA), under cooperative agreement with the National Science Foundation.

 0004-6256/94/108(2)/476/15/$0.90

as spiral arm kinks, gaps, spurs, bifurcations, endpoints to star formation ridges, dust-lane crossover points, interarm star formation, the ends of a weak bar, if present, or the location of the outermost H II region. These kinds of features have been used by Elmegreen & Elmegreen (1990) to estimate the pattern speed in the nearby spiral NGC 1566.

Resonance rings in barred spirals are more identifiable and thus more promising indirect tracers of the pattern speed than the features seen in grand-design spirals. These ring patterns are commonly found in what Buta (1986a) refers to as "ringed galaxies," i.e. galaxies of de Vaucouleurs types SB(r), SAB(r), (R)SB(r), (R′)SB(rs), etc.[2] The idea that rings could be definitive resonance tracers was beautifully demonstrated by Schwarz (1979, 1981, 1984, 1985) from a set of test-particle simulations. As noted by Kalnajs (1992), the locations of the rings in the models are not sensitive to the details of the underlying galaxy nor the complicated gas dynamics that produced them. To use rings to estimate pattern speeds, all one needs to know is the location of a ring, the resonance with which it is likely to be associated, and some kinematic information, such as a rotation curve or a two-dimensional velocity field.

In this paper, we will present a slightly different viewpoint from these previous studies. Rather than attempting to use rings or any other features to measure *specific values* of pattern speeds, we will compare new numerical simulations of barred galaxies with images and color index maps of representative early-type ringed galaxies in order to highlight different "pattern speed domains" among normal galaxies. It is not the actual value of a pattern speed that is important, but rather which resonances this pattern speed allows in a given disk. We find that we can understand a great deal about galaxy morphology by considering these domains and trying to match galaxies to simulation frames. For this purpose, we have constructed a new set of test-particle simulations that go beyond the work of Schwarz. We will show that the pattern speed could be one of the principal determinants of the large spread in morphologies seen among early-type disk galaxies (e.g., see de Vaucouleurs 1959).

2. SIMULATIONAL/OBSERVATIONAL DATABASE STRATEGY

The strategy in this paper is to compare simulation frames of a barred galaxy model to actual ringed, barred galaxies covering a range of observed morphologies. For this purpose, we take advantage of a library of *BVI* CCD images of ringed galaxies obtained by Buta and Crocker since 1990. The galaxies in this library are selected from the *Catalogue of Southern Ringed Galaxies* (CSRG; see Buta 1991a, 1993), which is a large database of morphologies, ring diameters, axis ratios, and bar/ring position angles for more than 3500 galaxies as seen on the SRC-J and ESO-R sky surveys. The catalogue was inspired by the work of Schwarz (1979, 1981) and was designed explicitly to test the resonance hypothesis of the nature of the rings. The image library includes the best examples of various bar and ring morphologies yet identified in the southern sky (see Buta & Crocker 1991). The images were obtained with CCDs at Cerro Tololo Inter-American Observatory (CTIO), Kitt Peak National Observatory (KPNO), and the Lowell Observatory.

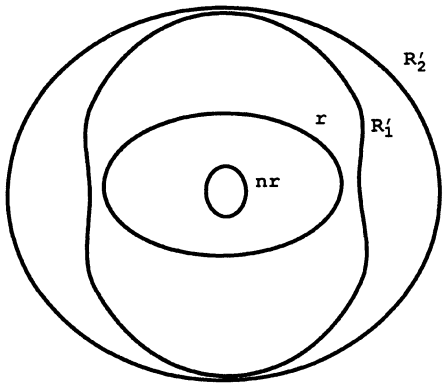

FIG. 1. Schematic diagram of periodic orbits near resonances with the bar pattern speed and probable associated ring types. The notation is as follows: **nr**, nuclear rings, associated with the inner Lindblad resonance where $\Omega_b=\Omega-\kappa/2$; **r**, inner rings, associated with the inner 4:1 resonance where $\Omega_b=\Omega-\kappa/4$; and **R**, outer rings, associated with the outer Lindblad resonance where $\Omega_b=\Omega+\kappa/2$. A prime indicates a pseudoring made of spiral arm segments. The two outer pseudoring types R_1' and R_2' are described in the text.

In comparing simulations with images, we will be using specific nomenclature and terminology for the various kinds of rings (see Fig. 1). Three classes of rings are seen in normal barred galaxies: inner rings **r**, which usually just envelop the bars in barred spirals; outer rings **R**, which are large, low surface brightness structures in the outer disk regions; and nuclear rings **nr**, which are small, high surface brightness structures found in the nuclei of barred and oval galaxies (see Buta 1990a for a review). The size ratios of the rings average 20:10:1 for the sequence **R**:**r**:**nr** (Buta & Crocker 1993). In addition to closed rings, there are pseudoring versions of each ring type where the feature is formed from spiral arms that close or are tightly wound. The nomenclature for these is **R′**, **rs**, and **nr′** for outer, inner, and nuclear pseudorings, respectively, following de Vaucouleurs (1959) and Buta (1989). In this paper, we will use the term "ring" in a generic sense to refer to both true rings and pseudorings.

Schwarz simulated the behavior of gas clouds in two-dimensional bar potentials imposed on the axisymmetric potential of galaxy disks. The gas clouds collided inelastically to form spiral shock fronts, which evolved relatively quickly into pseudoring and then closed ring features. It was possible to readily associate the kinds of rings which formed in the models to real galaxy rings. Schwarz suggested that outer rings are naturally interpreted in terms of the OLR, inner rings in terms of the inner second harmonic resonance (UHR), and nuclear rings in terms of an inner Lindblad resonance (ILR). These associations become even more likely when we consider that real inner, outer, and nuclear rings are

[2]Tilted rings created by the tidal disruption of small companions ("polar ring galaxies") and those formed by small companions plunging through a galaxy's disk ("ring galaxies") are not considered here and are much rarer than the rings we will be discussing.

typically bluer than the rest of the disk, indicating they are areas of gas aggregation and star formation, and have shapes and orientations in agreement with the predicted rings (Buta 1986a, b; Buta & Crocker 1991, 1993).

In addition to these usual categories, we will be referring frequently to subclasses of outer rings and pseudorings whose morphologies resemble those of simulated rings which formed near the OLR in the models of Schwarz (1981). These have recently been described in detail by Buta & Crocker (1991), who use the terminology $\mathbf{R}_1'$ for pseudorings which show a 180° winding of the spiral structure with respect to the bar ends, and $\mathbf{R}_2'$ for another variety which shows a 270° winding. A combined variety, referred to as $\mathbf{R}_1\mathbf{R}_2'$, is much rarer than these pure classes and was not predicted by Schwarz. Figure 1 of Buta & Crocker (1991) shows a schematic of all these varieties.

The prediction and subsequent identification of the OLR morphologies in large numbers of barred galaxies is an important advance in studies of internal galaxy dynamics. In the original models of Schwarz (1981), the two main OLR subclasses were linked to differences in the initial particle distributions in the models. One of our goals is to establish whether other, more physical conditions might be linked to the preference of one type over the other.

3. THE NEW SIMULATIONS

In our new simulations, we use a similar combination of an analytical two-dimensional barred potential and colliding test particles, or "gas clouds." The present code is derived from the self-consistent n-body code originally applied in studies of interaction-induced bar formation and gas flows (Salo 1991). In one set of simulations, the potential we use is the same that Schwarz (1981, 1984) used in his simulations. It is made of two parts, an axisymmetric isochrone potential and a bar. The isochrone potential has the form

$$\phi = -\frac{1}{1+\sqrt{1+r^2}}$$

which yields a rotation curve that rises to a maximum speed of ~0.4 at 2.2 program units from the center and then declines at greater distances [see Fig. 2(a)]. The standard Lindblad precession frequencies for this rotation curve are shown in Figure 2b. Here, Ω is the circular angular speed of rotation and κ is the radial epicyclic frequency.

Because most galaxies have flat rotation curves extending to large distances, and to determine the sensitivity of our results to the form of the rotation curve, we also carried out some simulations with the second rotation curve shown in Fig. 2(a). The form of this rotation curve is (Elmegreen & Elmegreen 1990):

$$V = \frac{kr}{r^A + r^{(1-\alpha)}}$$

where $A=-0.5$ and $\alpha=0$. The constant, k, was set to 0.42 so that the rotation velocity, V, reached about the same maximum value as the isochrone rotation curve. This rotation curve maintains a nearly constant level at large radii and is adequate for our purposes of simulating early Hubble type ringed galaxies. The Lindblad precession frequencies for this rotation curve are shown in Fig. 2(c).

For both the isochrone and flat rotation curve models, the bar potential has the form:

$$\phi_b = -0.53q[(r/a)^2 - 2.5(r/a)^4 + 2.1875(r/a)^6 - 0.65625(r/a)^8]\cos 2\theta$$

for $r \leqslant a$.

$$\phi_b = -0.16563q(r/a)^4 \cos 2\theta$$

for $r > a$. The values of the parameters a and q were chosen so that the relative radial force due to the bar would reach its maximum, usually 10%, at the distance which is 0.83 times the corotation radius. We tested for the effects of different bar strength with simulations using twice and half the 10% bar strength assumed above. We assume different pattern speeds of the bar potential in our simulations. For more details see Schwarz (1984).

The orbit integrations were made using a leapfrog method. The time step adopted was sufficiently small that there would be enough steps per rotation period to accurately follow the particles even in the inner regions of the system. For example, in the simulations with low bar pattern speed, 500 steps per bar rotation were used. We also checked that halving the step size did not affect any of the structures.

In Schwarz's simulations, two gas clouds collided inelastically when they were approaching and within the same box of a grid (suitable for a continuous gas). Because it has since been determined that most of the disk gas mass in our Galaxy is in the form of cold molecular clouds (e.g., Solomon & Sanders 1986), we instead follow the clouds' motions to determine when they approach to within the cloud radius and collide. The cloud radius we assume is $2\times10^{-3}\ r_{CR}$ where r_{CR} is the radius of corotation with the bar pattern speed. Again, we tested the sensitivity of our results to this parameter by carrying out simulations with smaller cloud radii and also without any collisions at all.

We also use more gas cloud particles (10 000 or more versus 2000 for Schwarz). Also one should note that Schwarz (1981) took advantage of the symmetry of his simulations about the bar and plotted 2000 mirror image pairs in his simulation images. Since our particle number approaches the actual number of clouds which comprise most of the gaseous mass, we do not do this reflection. Instead, we simply plot the individual particles. Because we do this, the reader can check the statistical reality of any feature by looking at the corresponding point diagonally opposite the center of the model. Because of the limited number of massive clouds in a real galaxy, this statistical variation from one side to the other will be present. The initial distribution of the clouds is of constant surface density out to r_1 which is slightly larger than r_{CR}. Thereafter the surface density falls linearly out to r_2 which is slightly larger than r_{OLR}, the outer Lindblad resonance radius.

The collision search method is an improvement over what Schwarz used in that the time of each collision is tracked. In the beginning of each step a collision search is done for each

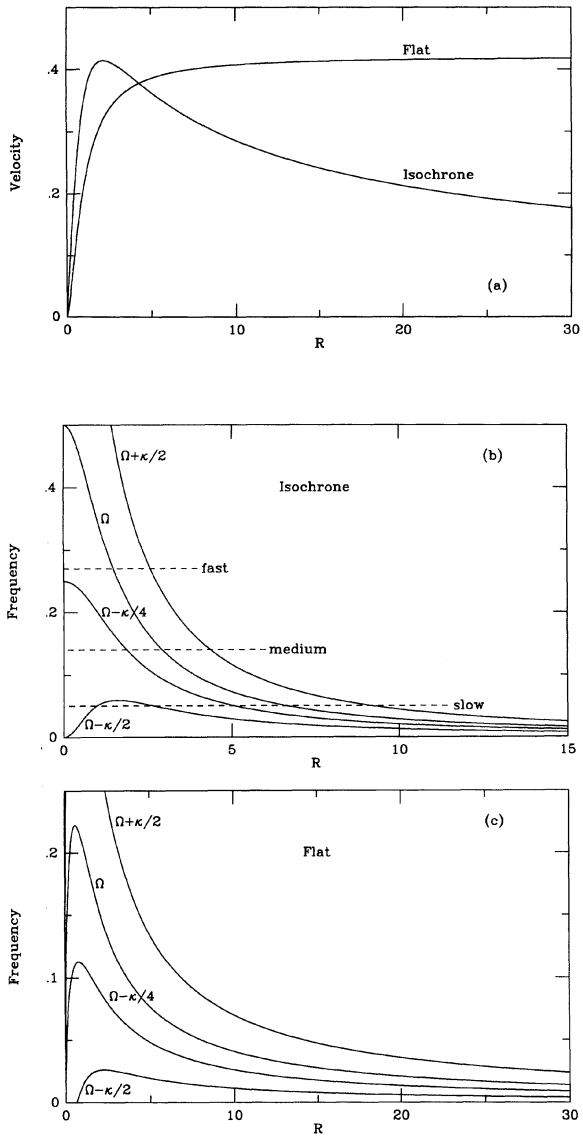

FIG. 2. (a) The rotation curves used for the simulations. (b) Circular angular velocity (Ω) and Lindblad precession frequencies ($\Omega \pm \kappa/m$) vs radius for the isochrone rotation curve. The three horizontal lines indicate pattern speeds in the fast, medium, and slow bar domains discussed in the text. Resonances occur where the pattern speed line intersects the frequency curves. (c) Same as (b) for the flat rotation curve model.

cloud particle. If a collision occurs, the relative velocities of the colliding particles are changed as follows:

$$v_r' = -\alpha v_r,$$

where v_r is the component of the relative velocity in the direction joining the two cloud particles before the collision and v_r' is the component afterward. The coefficient of restitution, α, is set to 0.2, an empirically reasonable value chosen to prevent the too rapid aggregation of the clouds over the duration of the simulation. As a result of these inelastic collisions, a spectrum of mass aggregates naturally forms ranging from loosely bound large aggregates down to the single cloud units.

The approach we have outlined is admittedly simplistic because a real galaxy has many more clouds than we are using, and these clouds cover a wider ranger of sizes. However, because the code is not very viscous, this has little consequence on our results. To give an idea of the physical time scales of our simulations, we take the co-rotation radius of our bar to be 5 kpc and the orbital speed at this radius to be 200 km/s. This gives the orbital period and thus the bar turning period to be about 150 million years. Under this physical scaling, the radius of our clouds would be about 10 pc which is observationally reasonable [but see Verschuur (1993) for a discussion of the problems of deriving meaningful diameters of clouds from H I observations]. The clouds were given an initial velocity dispersion of about 0.05 of their circular orbital velocity or about 10 km/s in our example here. This value is about the same as observed for clouds in our Galaxy.

4. RESULTS OF ISOCHRONE SIMULATIONS

4.1 Definition of Pattern Speed Domains

We carried out a simulation grid of individual frames with time at different bar pattern speeds as indicated in Figs. 3(a) and 3(b) for the isochrone rotation curve. For each simulation, shown in a horizontal sequence of frames, the fixed bar pattern speed, Ω_b, is indicated on the lower left of the first frame. The time of the frame in bar rotations is given on the upper left of each frame. The bar is always horizontal in each image. The reader can determine which resonances occur in each simulation by setting a horizontal ruler at the simulation pattern speed in Fig. 2(b). We will refer to a "fast" bar as one whose pattern speed is high enough to avoid both a UHR and an ILR [upper horizontal line in Fig. 2(b)]; a "medium" bar as one whose pattern speed allows a UHR but not an ILR [middle horizontal line in Fig. 2(b)]; and a "slow" bar as one whose pattern speed allows both a UHR and an ILR [lower horizontal line in Fig. 2(b)]. All pattern speeds allow an OLR. Figure 3(c) shows the last frames of Fig. 3(b) enlarged.

4.2 R_1' vs R_2' Outer Pseudorings

As we have noted, in Schwarz's work the R_1' and R_2' morphologies resulted from differences in initial particle distributions. When the initial disk was loaded with particles that did not extend much beyond the OLR, the inner, perpendicular-aligned OLR orbit family was preferred and an R_1' pseudoring resulted. However, with a more uniform gas distribution that extended beyond the OLR, the outer, parallel-aligned OLR orbit family was preferred and an R_2' pseudoring resulted (see Figs. 4 and 10 of Schwarz 1981). Schwarz also found that the R_2' rings were more robust than the R_1' rings and therefore more likely to be observed. However, preliminary analysis of CSRG data suggests that R_1' rings are the most common variety in SB galaxies (Buta 1986a).

Our isochrone simulations give a different picture of the conditions required for formation of the two OLR pseudoring types. Duplicating Schwarz's experiments, we have tried

simulations where the particles are all inside the OLR, and simulations where the particles extend beyond the OLR. Contrary to Schwarz, we find that R_2' rings can form under either circumstance. The difference in these results is due to our using more particles, tracking collisions more accurately, and running simulations for more bar rotations than did Schwarz. Instead of a strong link to initial density distributions, we find that the appearance of either an R_1' or an R_2' pseudoring depends primarily on the value of the pattern speed and the time interval since the bar potential was imposed.

The age effect for the formation of the outer rings happens for both fast and slow pattern speeds in the isochrone potential. Over a wide range of pattern speeds, R_1' rings tend to form quickly and R_2' rings later when the R_1' rings may have dispersed. The highest pattern speed case that we considered in the isochrone potential has $\Omega_b=0.27$. This barely avoids a UHR according to Fig. 2(b). For this simulation in Fig. 3(a), an R_1' ring is present at early times. At later times, a strong R_2' pseudoring develops with a trace of an R_1 component aligned 90° to the bar still evident in the last time step (30 bar rotations). The pattern in this time step bears a strong resemblance to the observed R_1R_2' morphology discussed by Buta (1986a) and Buta & Crocker (1991), and is the first simulation we know of which generates this combined ring morphology. At slower pattern speeds than 0.27, only the R_2' ring is clearly visible at later times.

There are some initial distribution effects but they are less important than the time and pattern speed. For slow pattern speeds in the isochrone potential, such as the $\Omega_b=0.04$ simulation in Fig. 3, the initial R_1' ring is clear but the later R_2' is weak. However, in this simulation, the particle distribution ends at the OLR. Figure 4 shows the same simulation but with particles extending beyond the OLR. The placing of these particles in the ring forming region promotes the formation of a strong R_2' ring at low bar pattern speeds as can be seen in Fig. 4 at six bar rotations. Here we increased the number of particles to 20 000 with an initially wider and flat distribution.

5. SIMULATION RESULTS COMPARED TO OBSERVATIONS

We will now show observational examples that match our high, medium, and low pattern speed simulations. The close matches in these cases support the idea that bar pattern speed relative to the rotation curve may vary significantly among galaxies. Both high and low pattern speed galaxies should form R_1' and R_2' outer rings. For high pattern speeds, the absence of the inner resonances should lead to an absence of inner structure, such as an inner or nuclear ring, and bar dust lanes. The existence of these resonances leads to this inner structure at slower pattern speeds. Finally, different galaxies that have the same pattern speed may show morphological differences reflecting the time difference since the bar potential was imposed.

5.1 High and Medium Pattern Speed Examples

The spiral galaxy ESO 509-98, shown in the lower frame of Fig. 5, bears a strong resemblance to the $\Omega_b=0.22$ or 0.27 isochrone models at the latest time step. In addition to the bulge and disk, the galaxy has only a bar and an R_1R_2' spiral pattern that is completely detached from the bar. *There is no evidence for an inner ring or lens, or any nuclear structure, and no nuclear star formation* [see the $B-I$ color index map in Buta & Crocker (1991)]. The main point of disagreement between the morphology of the galaxy and the model is the population of the "banana" orbits seen in the $\Omega_b=0.27$ simulation. These orbits involve motion around the Lagrangian points L_4 and L_5 in the rotating reference frame. In ESO 509−98, the regions where these orbits would lie are clearly deficient in light. We will later show that if we increase the bar strength, the banana orbits become unstable and the region of the Lagrangian points almost clears of particles.

At slower pattern speeds, the inner structure begins to appear. The upper left panel of Fig. 5 shows NGC 2665, which resembles an early medium pattern speed stage, as at 5 bar rotations for $\Omega_b=0.10$ in Fig. 3(a). The galaxy has an excellent but slightly asymmetric R_1' pseudoring aligned nearly perpendicular to the bar in projection, a trace of an inner ring, but no offset bar dust lanes. The $B-I$ color index map in Buta & Crocker (1991) reveals a small blue nucleus.

At 10 bar rotations for $\Omega_b=0.10$, a closed, oval inner ring and an R_2' outer pseudoring have developed. A good possible example of a galaxy in this phase is ESO 325−28, shown in the upper right panel of Fig. 5. This object also has a blue nucleus like NGC 2665, but no strong offset bar dust lanes or a nuclear ring (Buta & Crocker 1991). Note the highly elongated and pointy shape of the inner ring in this galaxy, which is very similar to the model. Thus, NGC 2665 and ESO 325−28 may represent earlier and later stages of evolution at the same relative pattern speed.

5.2 Low Pattern Speed Examples

The new features that become prominent at low pattern speeds are strong inner rings or pseudorings associated with the UHR, shock fronts along the bar that initially resemble the offset dust lanes seen in many real bars, and circumnuclear rings of various shapes associated with one or two ILRs (see also Schwarz 1984).

Our improved simulation resolution in the center shows the nuclear ring in much more detail than Schwarz's models could reveal. Our nuclear rings are longer lasting, evolving from elongated shapes to more circular shapes and only slightly smaller sizes. For progressively smaller pattern speeds, we see first inner rings, then lanes in the bar which "feed" nuclear rings. We note that the model inner rings tend to be aligned parallel to the bar, but that model nuclear rings can have parallel, perpendicular, or intermediate alignments. These alignments are consistent with observations (see Buta 1986a; Buta & Crocker 1993).

The galaxy NGC 6782, type (R_1')SB(r,nr)0/a, embodies the essential features of what we consider to be a slow pattern speed barred galaxy. We display four images of this

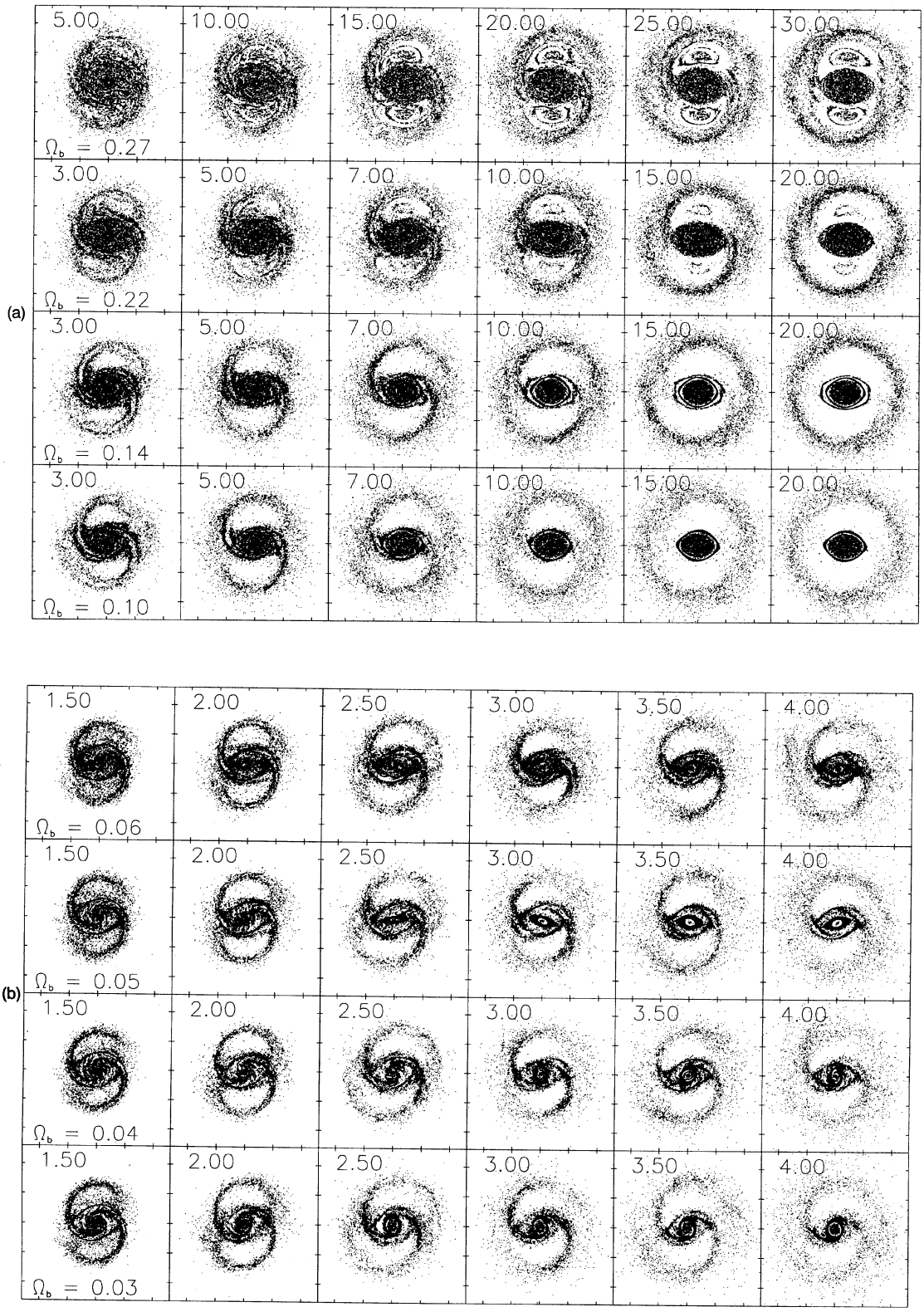

FIG. 3. A grid of simulations based on the isochrone potential. Bar pattern speed, Ω_b, is indicated on the lower left of the first frame and the time in bar rotations on the upper left of each frame. The bar is horizontal in all of the frames and has a strength of 10%. One axial tick mark interval corresponds to the radius of CR. The same is true for all of the other similar figures. In (a) and (b) we show the full time sequences over the adopted range of pattern speeds. In (c) we show closeups of the last frames in (a) and (b).

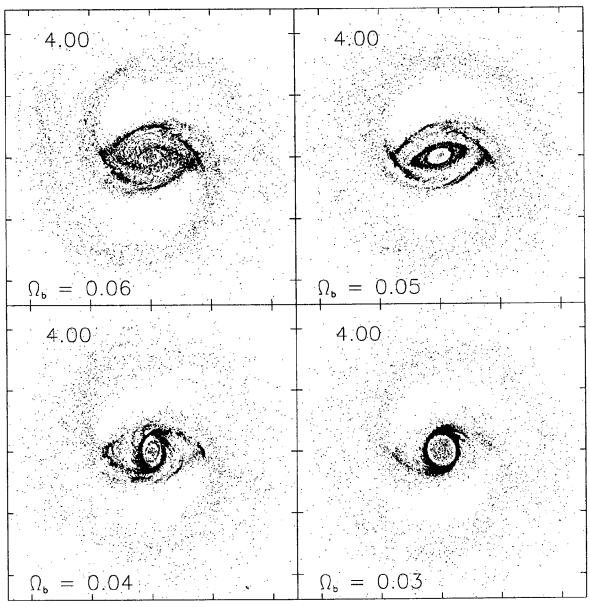

(c)

FIG. 3. (continued)

object in Figs. 6 and 7. The top panel of Fig. 6 shows a *B* band image which reveals the three main ring features. The inner ring is pointy and remarkably football shaped, and its apparent elongation along the bar axis cannot be due to projection effects because the R_1' feature is elongated more nearly perpendicular to the bar. The faint outer isophotes are rounder than either of these features (see lower panel of Fig. 6), so the inclination of the galaxy is probably not more than about 30°–40°. Figure 7 (top panel) shows a $B-I$ color index map of the central region and reveals clear leading dust lanes and blue inner and nuclear rings, the latter being rather circular. These structures resemble the features seen in the $\Omega_b=0.06$ simulation after 3.5 bar rotations. Even the weakness of the R_1' pseudoring in the quadrants leading the bar is evident in NGC 6782. The *I* band image in the lower panel of Fig. 7 reveals the only feature of this galaxy which is not readily explained by our models: a small secondary bar whose major axis trails the axis of the primary bar (see also Buta & Crocker 1993). This feature very likely formed from the buildup of a massive nuclear gas disk which formed its own bar instability and which decoupled gravitationally from the pattern speed of the primary bar (Pfenniger & Norman 1990; Friedli & Martinet 1993).

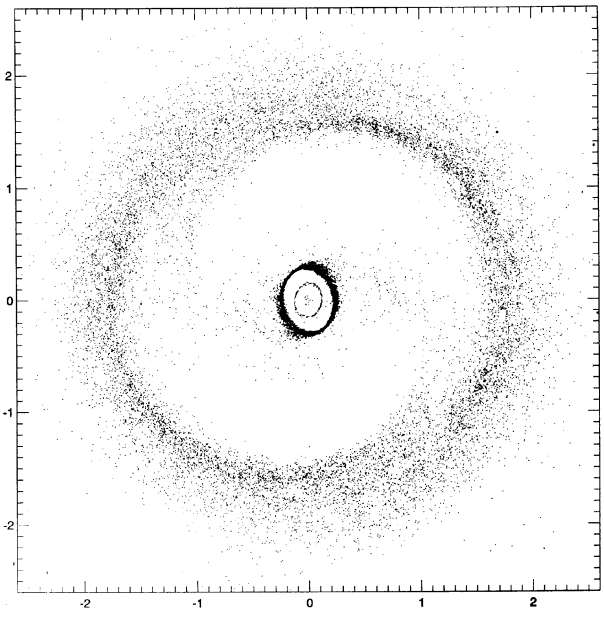

FIG. 4. The $\Omega_b=0.04$ simulation of Fig. 3 but at six bar rotations and with an extended distribution of 20,000 particles.

In Fig. 3(b) and in the enlargements in Fig. 3(c), it is interesting how the offset shock fronts in the $\Omega_b=0.06$ and 0.05 simulations evolve to a closed nuclear ring highly elongated nearly along the bar, while in the $\Omega_b=0.04$ and 0.03 simulations, the nuclear ring is more circular and nearly elongated perpendicular to the bar. The difference could be due to the increasing importance of the x_2 family of periodic orbits with decreasing pattern speed (Contopoulos & Grosbol 1989). Neither the central regions of NGC 6782 nor those of other nuclear-ringed galaxies displayed or compiled by Buta & Crocker (1991, 1993) resemble the nuclear feature which develops for $\Omega_b=0.05$.

The shape and size of the nuclear rings in our simulations are very sensitive to the form of the rotation curve near the center. Most simulations in this paper have a gently rising curve near the center and produce large nuclear rings [D(OLR)/D(ILR)≈5–6]. Of 20 nuclear rings in SB galaxies listed by Buta & Crocker (1993), only one, that in ESO 565−11, has a relative size this large. The more typical barred galaxy has a ratio D(R)/D(nr) closer to 20. When we use a more steeply rising curve in our simulations, the model nuclear rings become smaller.

5.3 The Sequential Formation of the Types of Rings

Our models have revealed a time sequence associated with outer ring formation. In all pattern speed simulations, R_1' rings form first and then evolve later into R_2' rings. Although we believe we can identify galaxies in such different evolutionary states at the same relative pattern speed (as in NGC 2665 and ESO 325−28 in Fig. 5), further evidence in support of the time sequence is essential. We believe we have found such evidence in the large CSRG galaxy IC 1438, type (R_1R_2')SAB(r,nr)0/a (Fig. 8). This galaxy is a rare example having four ring types. It is an excellent example of the R_1R_2' morphology, like ESO 509−98 (see Fig. 5). However, unlike this latter object, IC 1438 has excellent inner and nuclear rings as well as bar dust lanes (see lower panel of Fig. 8, which is a $B-I$ color index map). It cannot be a fast bar case such as ESO 509−98 because of the existence of the inner and nuclear rings. An interesting aspect of the galaxy is that *the R_1 component is most prominent in the infrared (see right panel of Fig. 8) while the R_2' component is most prominent in the blue (see left panel of Fig. 8)*. This presumably reflects an age difference between the two components. The suggestion is that the R_1 part formed first and

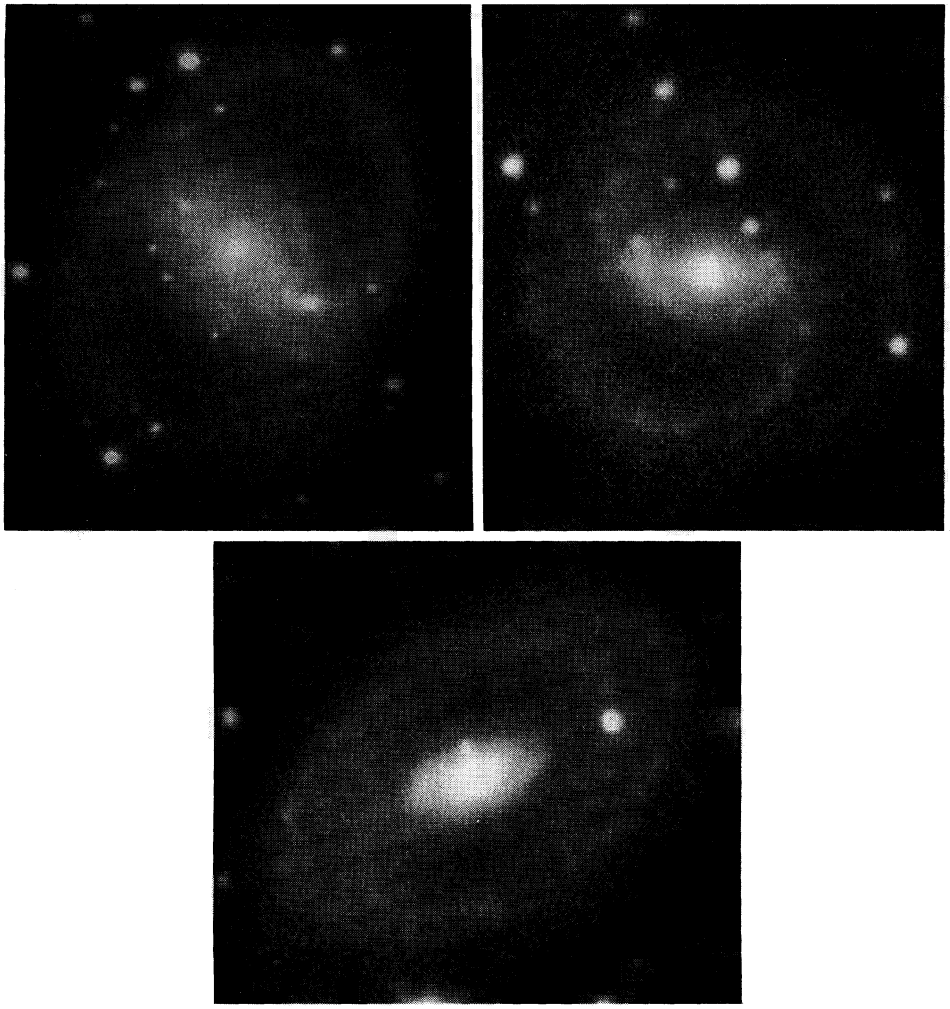

FIG. 5. Three CSRG galaxies which resemble medium and fast pattern speed simulations (see text). The galaxies are NGC 2665 (upper left), ESO 325−28 (upper right), and ESO 509−98 (lower middle). These images and all others in this paper are based on observations made at CTIO with a TI or TEK 1024 CCD chip. The images are logarithmic, sky-subtracted, and in units of mag arcsec^{-2}. The range displayed is from 18.0 to 28.0 mag arcsec^{-2}.

may have lasted long enough to leave behind a stellar remnant containing stars trapped in the R_1 periodic orbit family. At the present time most of the gas is associated with the R_2' part, and there is still some gas associated with the inner and nuclear rings since these are also blue enhancements in the $B-I$ color index map. The time sequence seems consistent with our simulations, and the gaseous structure resembles the frame for $\Omega_b=0.06$ at 4.0 bar rotations.

All of the above simulations used colliding clouds which dissipated energy in collisions. However, we find that outer and inner rings are not very sensitive to the number of collisions, as shown in Figs. 9(a)–9(c). The first of these figures has clouds 1/5 the normal size. The second has no collisions at all. A comparison of these two figures to Fig. 3(b) for $\Omega_b=0.04$ at four bar rotations shows that our results are not sensitive to the exact frequency of collisions. These simulations started the noncolliding particles in circular orbits with very small velocity dispersion. The stars in an early type galaxy disk would have a much larger velocity dispersion, so we emphasize that this simulation does not indicate that resonance rings can form from pre-existing disk stars. We show this in Fig. 9(c) where the initial velocity dispersion is set to the value 0.25 of the circular velocity, the dispersion we would expect for a stellar component in an early type galaxy.

5.4 A Connection between Nuclear Rings, Dust lanes, and R_1' Pseudorings?

We have found that both nuclear and R_1' rings are created by low pattern speed bars with R_2' rings being weaker, only appearing after a longer time span. The strongest R_2' rings are created more quickly at the highest pattern speed where no nuclear ring forms. This leads to a prediction that has already found some observational support. *We expect that nuclear rings will be associated more often with R_1' pseudorings than with R_2' pseudorings.* There is preliminary observational evidence of just such a correlation. Buta & Crocker (1991) found that of 11 galaxies with definite R_1' rings, 9 show

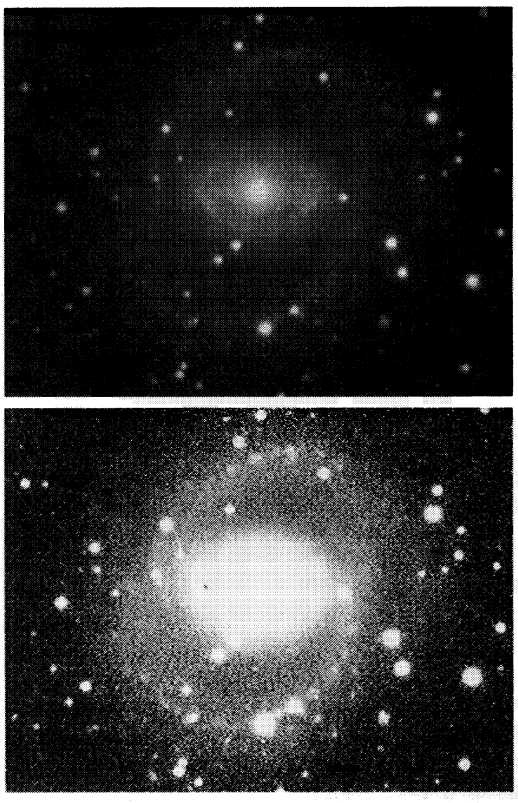

FIG. 6. Images of NGC 6782, a CSRG galaxy which resembles the slow pattern speed simulations for Ω_b=0.06 in Fig. 3. The panels are: (top) *B* band showing the three ring features: a nearly circular nuclear ring, a pointy oval inner ring, and a faint R_1' outer pseudoring; (bottom) deeper *B* band to show the more circular outer isophotes.

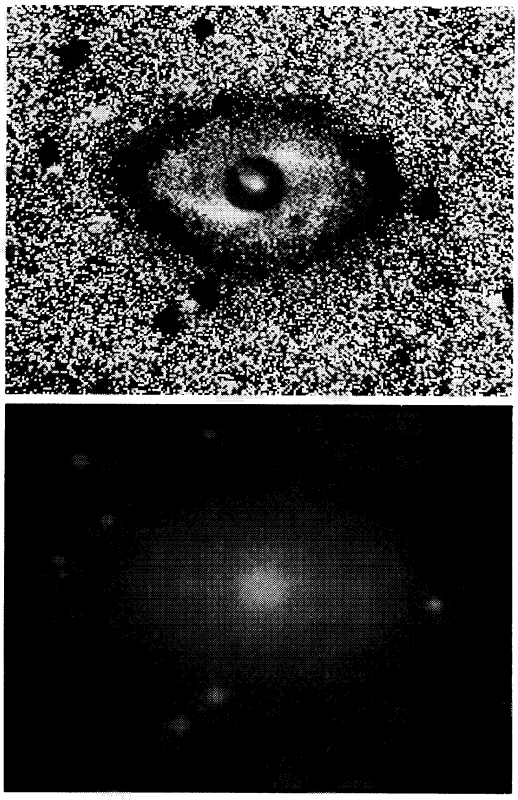

FIG. 7. Images of the central regions of NGC 6782: (top) $B-I$ color index map, coded such that blue features ($B-I\approx1.0$) are dark and red features ($B-I\approx3.0$) are light; note how star formation concentrates in the inner and nuclear rings, and the strong leading dust lanes in the bar; (bottom) *I* band image of the inner regions showing the secondary bar which lies inside the nuclear ring; this feature is one of the best examples of a "trailing" nuclear bar (see text). This feature is not explained by the simulations in Fig. 3.

evidence of nuclear star formation and offset bar dust lanes. Conversely, of 11 galaxies with definite R_2' rings, only 3 show evidence of nuclear star formation or bar dust lanes. Crocker & Buta (1993) have confirmed the correlation with more galaxies and have used *IRAS* data to quantify it in terms of the far infrared to blue luminosity ratio.

6. EFFECT OF DIFFERENT BAR STRENGTHS

Figure 10 shows two simulations (Ω_b=0.27 or Ω_b=0.04, respectively) which are the same as Fig. 3 but with the bar strength increased to 20% in the two left frames and decreased to 5% in the two right frames. The reader will note that in some of the fast pattern speed simulations of Fig. 3, banana shaped loops appear above and below the bar. This happens only for the fast pattern speeds. Confirming Schwarz (1984), we have found that if the bar is strengthened these disappear.

We also find an effect predicted analytically by Contopoulus & Grosbol (1989). The reader will note that in the stronger bar (left) portion of Fig. 10 the nuclear ring is parallel to the axis of the bar whereas in the weaker bar (right) portion, the ring is perpendicular to the bar axis. This is probably because the x_2 family of orbits has become unstable in the strong bar case. (These orbits are stable in the Fig. 3 simulations.) Also as the bar is weakened the inner ring becomes more circular and no strong outer ring feature forms.

7. ALTERNATIVE HYPOTHESES FOR MORPHOLOGY DIFFERENCES

Up to now we have assumed that the bar pattern speed varies sufficiently relative to the rotation curve that some galaxies have all the major low-order Lindblad resonances while others only have some. However, we have not discussed what determines the bar pattern speed, at least initially. Previous *n*-body models of bar formation (Sellwood 1981; Combes & Sanders 1981; Sparke & Sellwood 1987; Combes & Elmegreen 1993) suggested that during the collapse phase, the initial pattern speed could avoid an ILR if the central mass concentration is not too high. These models also found that, after the collapse phase, the pattern speed would decrease with time, and eventually ILRs would be allowed, especially for early Hubble types with large bulge to disk ratios. In a study of several early type barred galaxies with apparent isophote twisting in the nucleus, Shaw *et al.*

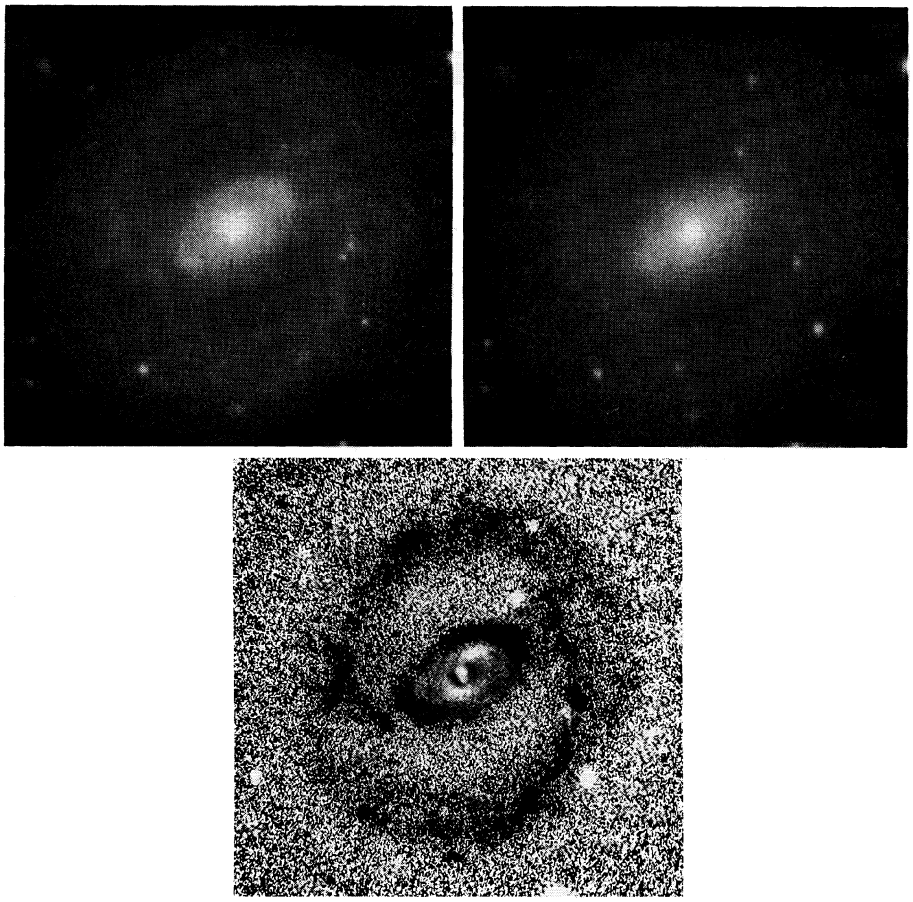

FIG. 8. Images of IC 1438, a CSRG galaxy with four different ring and pseudoring types. The upper left panel is a *B* band image which shows a prominent R_2' outer pseudoring and a pointy oval inner ring. The upper right panel shows an *I* band image; in this passband, the outer structure is dominated by a virtually detached R_1 component. The lower panel shows a $B-I$ color index map which is coded the same as in Fig. 7. This map best reveals the nuclear ring and the offset leading bar dust lanes. The nuclear ring, the inner ring, and the R_2' part of the outer regions appear to include gas dynamics and recent star formation. The R_1 component is clearly dominated by older stars than in these other features.

(1993) suggested that the final pattern speed of the bar would be close to the weighted average of the $\Omega-\kappa/2$ curve over the bar length, which would be limited mainly by the corotation resonance. All the resonances would thus be present in every early type barred disk galaxy. To avoid the nuclear and inner rings in the present morphology, the gas would have to be consumed rapidly enough in these regions that there would be little or no current star formation. One would nev-

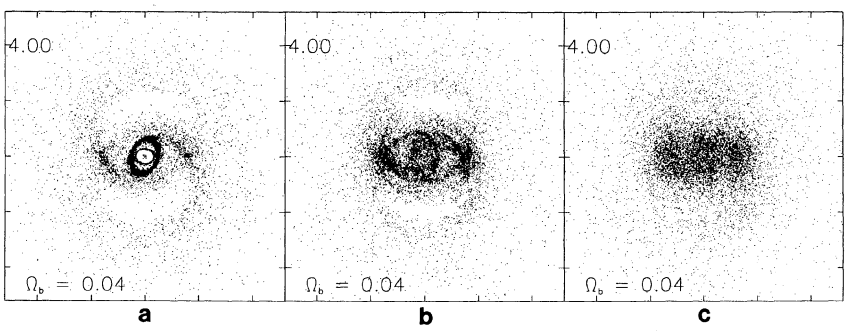

FIG. 9. (a) A time frame of a Fig. 3 simulation in which the gas clouds are only 0.2 times the normal size. In this case collisions occur at a much smaller rate. (b) A time frame of a Fig. 3 simulation in which the gas clouds do not collide. (c) A time frame of a simulation illustrating the effect of the bar on the stellar component of the disk. This frame also matches Fig. 3 except that collisions do not occur and the velocity dispersion is larger.

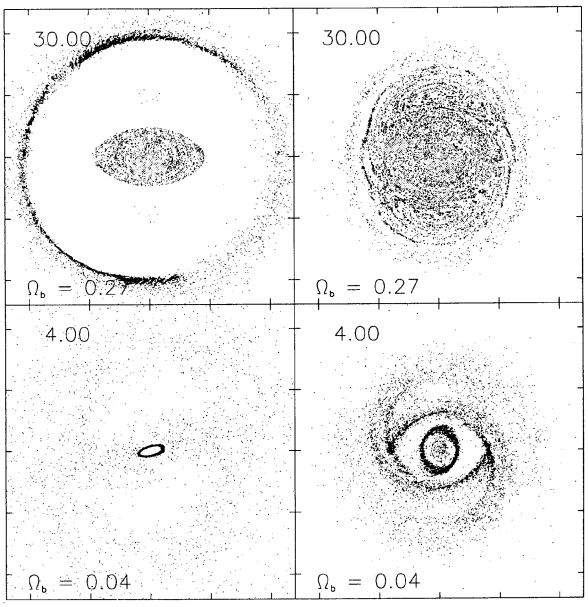

FIG. 10. The effect of bar strength on fast and slow bar cases. For each pattern speed shown, the left frame has a bar twice as strong as the corresponding model in Fig. 3, while the right frame has a bar half as strong.

ertheless expect that there would still be some trace of those features, either in the form of a diffuse lens around the bar, a nuclear lens, a nuclear bar, or a triaxial bulge (see, e.g., Buta 1986b; Pfenniger & Norman 1990). However, we do not see such features in the bar region of ESO 509−98. In this circumstance, one could then argue that some galaxies did not have a sufficient initial gas content or gas distribution to allow an old ring to develop at either resonance, or that velocity dispersion spreads out some rings to invisibility if no new stars have formed for a very long time.

This is a difficult problem to evaluate, but as a first step it is useful to try and estimate the frequency of high, medium, and low pattern speed galaxies. Of the galaxies in our image library, 79 have outer rings or pseudorings that can be subclassified into the R_1' or R_2' categories. These are the ones we can best evaluate in terms of our models. We emphasize that this sample consists mostly of galaxies in the de Vaucouleurs revised Hubble type range $S0^+$ to Sb, i.e., early-to-intermediate type spirals and late S0's. We have examined each of these galaxies in the context of Fig. 3. While some of these galaxies can be readily fit into our models, as we have shown, others cannot. The problem cases usually involve inner lenses instead of inner rings, very weak bars, nuclear bars in the absence of primary bar dust lanes or a nuclear ring, and possible evolved R_1 outer rings. In many cases, we could not make a reliable judgment because of these difficulties.

However, from inspection of all of our galaxies, we believe we can make one fairly accurate statement. In our entire image library, we find at most two galaxies that we believe definitely fit our view of a fast pattern speed galaxy. These are ESO 509−98 as described in Sec. *5.1*, and ESO 287−56. This latter galaxy (an image of which will be presented in a separate paper) consists of an excellent dimpled R_1' outer pseudoring and a bar, but has no trace of an inner ring or lens, or any nuclear feature. While ESO 509−98 would be a late, fast pattern speed example, ESO 287−56 would have to be an early one in the context of Fig. 3 (for example, Ω_p=0.22, T=7.0 bar rotations). It appears that fast pattern speed galaxies may have the lowest relative frequency of occurrence.

The remaining galaxies in our sample can all be placed into the medium or slow pattern speed categories over a range of times, depending on how we interpret inner lenses, dust lane patterns, and nuclear bars. As an example of the difficulties of these comparisons, we bring attention to cases like NGC 1291 (de Vaucouleurs 1975) and NGC 1543 (Jarvis *et al.* 1988). Each of these galaxies has an excellent detached outer ring, an inner lens, and a small secondary (or nuclear) bar. Though neither has an inner or nuclear ring, the presence of the secondary bar suggests nevertheless that an ILR is present (see Sec. *5.2.1*). Thus, we suggest that both are slow pattern speed, highly evolved examples where currently there seems to be little or no gas near the ILR and UHR.

Is there any evidence that bar pattern speeds actually decrease with time? If this does happen, such that ILRs appear late in the evolution, then we might expect rings in the initial fast pattern speed phase if the time scale for ring formation is shorter than the time scale for bar slowing. However, if this were the case the radius of a particular resonance ring would change with time. The galaxy NGC 7702 (Buta 1991b) is the only case where it has been possible to reliably separate the old and young components of a bright, mostly stellar inner ring to at least examine this question. Buta found that the inner ring has a narrow cross section in blue wavelengths (young stars) and a broader cross section in the red component. The colors of the broad component indicate a much greater age than for the narrow component, yet the radial positions of the two components are nearly the same. Does this mean the pattern speed has not changed much over the few billion year lifetime of this feature? This is unclear because, as noted by the referee, it is unlikely that the old ring can be left behind at an earlier radius of the resonance, as if it no longer felt the potential of the rest of the galaxy. This is a topic that we are further investigating. We note that the broadening of the red ring component compared to the blue one is straightforward to understand. Stars formed in the ring from gas clouds would continue to be confined in the family of periodic orbits constituting the inner ring if self gravity of the gaseous ring is unimportant. Some broadening should occur via dynamical scattering of the stars by the gas clouds in the ring (e.g., Mihalas & Binney 1981). Figure 9(b) is a simulation test of whether these formed stars will be confined. In the simulation, there are no collisions among the particles which are placed initially in a uniform disk. In fact, an inner ring does form and it is broader than the features which developed in the Ω_b=0.04 simulation in Fig. 3(b), where collisions do occur when the particles are taken to be gas clouds.

Figure 11 shows a simulation of another alternative hypothesis, that all the resonances are present but the gas dis-

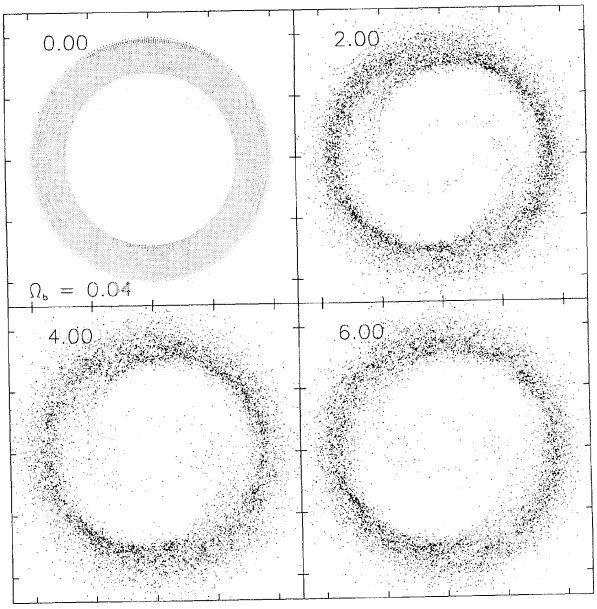

FIG. 11. A simulation of the hypothesis that all resonances are present but the gas lies mostly outside the OLR, thereby precluding the formation of nuclear and inner rings. In this case, a strong R_2' outer pseudoring develops. The number of bar rotations is in the upper left corner of each frame.

tribution precludes nuclear and inner rings, i.e., gas is only present in the outer parts of the galaxy. This is a possible but rather artificial alternative. However, it would be consistent with the preferential stripping of small gas-bearing satellite galaxies with orbits near the disk plane. The Holmberg asymmetry of satellites of edge-on spirals suggests that this could occur (Byrd & Valtonen 1987). In the Fig. 11 simulation, we initially placed all particles outside the OLR. Some of the clouds migrate inward past the OLR to form an R_2 ring then into the R_1 ring region. We see that there is a reasonable match with ESO 509−98 in Fig. 5 even down to the arm arcs coming inward from the outer ring toward the ends of the bar. However, this simulation is inconsistent with the time sequence for IC 1438 where the R_1 ring is older than the R_2 ring. Thus the gas distribution hypothesis is possible but not likely to be universal.

8. RESULTS OF FLAT ROTATION CURVE SIMULATIONS

The results of the flat rotation curve simulations are displayed in Fig. 12(a). In this figure, the sequences in the third and fourth rows have the same value of Ω_b, but the bar strengths are 10% and 20%, respectively. The layout is the same as in Figs. 3(a) and 3(b). For gauging pattern speed domain, the reader should refer to Fig. 2(c). In this case, the Ω_b=0.12 simulation is in the fast bar domain, while the Ω_b=0.03 simulation is in the medium to slow bar domain. As for the isochrone simulations, we find the development of gaseous rings near the allowed low order orbit resonances. The rings are most prominent for the Ω_b=0.03, 20% bar strength sequence in the lower row of Fig. 12(a). This simulation also shows a multiarmed pattern near the inner ring that strongly resembles what is seen in some ringed, barred galaxies. An example, NGC 1433, is shown in Fig. 13. The last frame in the bottom line of Fig. 12(a), shown enlarged in Fig. 12(b), lower right, matches some of the features of this excellent ringed galaxy, including the secondary arcs positioned off of the leading edges of the bar.

An obvious difference between the Fig. 12 and Fig. 3 simulations is the lack of development of any R_2' features in Fig. 12. This is because the flat rotation curve simulations have not been carried to a sufficient number of bar rotations. The Fig. 12 Ω_b=0.12 simulation after 10 bar rotations is very similar to that in the isochrone Ω_b=0.27 simulation after the same number of bar rotations. This shows that when comparing simulations, one must gauge the pattern speed domain first, and then compare frames after a similar number of bar rotations.

9. CONCLUSIONS

By means of using many more simulations than Schwarz, improving his method of tracking collisions, and adding many more cloud particles, we have obtained rather good qualitative matches of simulations with observed galaxies. We have followed the procedure suggested by Sellwood & Wilkinson (1993) of conducting many simulations with different bar pattern speeds to obtain morphological matches with observations. The simulations suggest that we could identify high, medium, and low pattern speed (with respect to the rotation curve) galaxies using the following criteria:

(1) Any galaxy showing an outer ring or pseudoring but *no trace* of an inner ring, offset bar dust lanes, a nuclear ring, or any features normally associated with nuclear rings such as a nuclear bar, would be a candidate for a fast pattern speed case.

(2) Any galaxy showing an outer ring or pseudoring and an inner ring or pseudoring, but no trace of offset dust lanes, a nuclear ring, or any features normally associated with nuclear rings such as a nuclear bar, would be a candidate for a medium pattern speed case. Depending on the relationship between inner rings and inner lenses, the presence of the latter could also signify a medium pattern speed case.

(3) Any galaxy showing outer, inner, and nuclear rings or pseudorings simultaneously would be a clear candidate for a slow pattern speed case. However, the presence of a nuclear bar (or triaxial bulge), even if no nuclear ring is present, could still signify a slow pattern speed.

These rules could be invalidated by an interaction with a neighboring galaxy. But we realize also that gas depletion could invalidate the use of a nuclear ring to infer pattern speed domain. If the final pattern speed of a galaxy is determined by the shape of the potential, as suggested by Shaw *et al.* (1993), then most galaxies would be in the slow domain whether they currently show nuclear rings or not. The time scale for gas consumption in the nuclear ring could be one or two orders of magnitude shorter than in an outer ring (e.g., Combes & Gerin 1985; Kenney *et al.* 1993). However, since we also use (1) the absence of an inner ring or lens, and

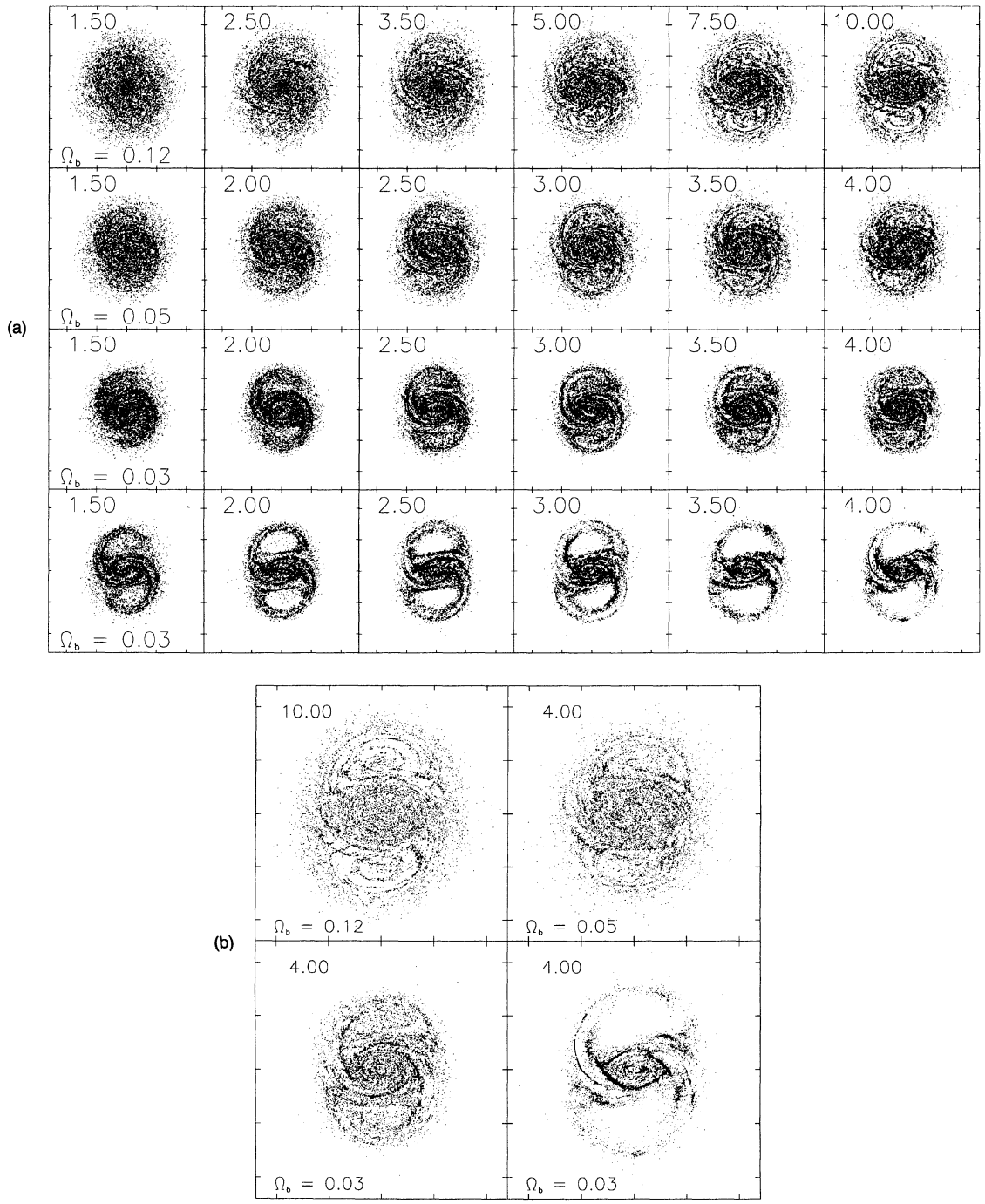

FIG. 12. (a) A grid of simulations based on the flat rotation curve. The layout and labeling are the same as in Fig. 3. In the first three rows, the bar strength is the same as in Fig. 3, while in the lowermost frame the bar strength is 20%, or twice that in Fig. 3. (b) The last frames of each of the simulations in Fig. 12(a) are shown enlarged.

(2) the absence of a nuclear bar or triaxial bulge, as diagnostics for high pattern speeds, the absence of a nuclear ring would merely provide a consistency check.

We have identified an interesting set of patterns among the observations and among the simulations. Schwarz (1981) simulated the behavior of gas clouds in two-dimensional bar potentials turning at a given pattern speed relative to the disk material's orbital motion. Outer rings were first found by Schwarz who attributed them to two different families of periodic orbits near the outer Lindblad resonance of the bar. Schwarz found that R_1' and R_2' pseudorings were favored by different initial particle distributions. In improved simulations which use more particles and track cloud collisions more accurately, we instead find that bar pattern speed and

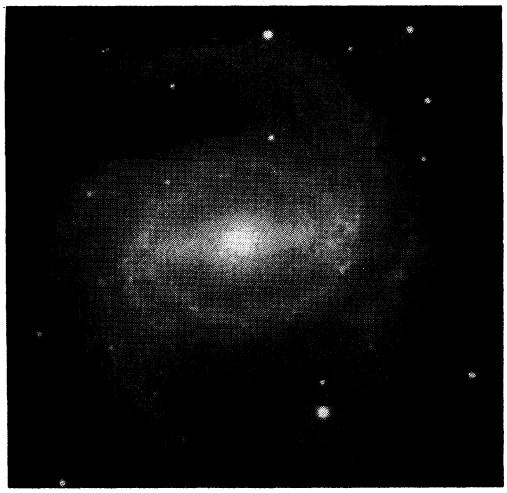

FIG. 13. Illustration of NGC 1433 which matches a frame of the flat rotation curve grid in Fig. 12(a) and the lower right enlarged frame of Fig. 12(b).

to a lesser extent time evolution at a given pattern speed determine whether one or the other type of outer ring is seen. For each pattern speed, our models yield R_1' outer pseudorings at earlier times and R_2' or combined R_1R_2' outer pseudorings at later times. For low pattern speeds, we obtain inner rings and/or nuclear rings in addition to outer rings or pseudorings. We do find some effects of particle distribution. If particles initially are found in the R_2' region, this ring forms faster. The appearance of the patterns is also mildly sensitive to the form of the rotation curve, and more so to the bar strength.

Using a comprehensive database of multicolor images of selected ringed galaxies, we find that the observed properties and occurrence of the different ring types are consistent with our simulation results. Some galaxies match our simulations very well. We find that galaxies with R_2' outer pseudorings tend not to have inner rings or nuclear rings similar to our fast pattern speed simulations. Galaxies with R_1' outer pseudorings tend to have inner rings and nuclear rings similar to our medium and slow pattern speed simulations. These results suggest that resonance ring galaxies do actually have a variety of bar pattern speeds relative to the rotation curve. However, there is an indication that fast pattern speed galaxies are rarest. We suggest that the large spread in morphology at a given Hubble type, especially among early types (de Vaucouleurs 1959), is due in part to pattern speed differences among galaxies of similar mass. The way to test this idea further would be to obtain rotation curves or two-dimensional velocity fields of the best examples of each apparent pattern speed domain, and then determine whether or not inner resonances should exist. This would be nontrivial for early type ringed galaxies, since it would require both gaseous and stellar rotation data, but is currently feasible. We have obtained kinematic data for a few of our sample galaxies that will be presented in future papers.

There is considerable evidence that companions play a role in bar formation. Elmegreen *et al.* (1990) have found that there is an observational correlation between whether a galaxy is barred and whether companions are nearby. The angular rate of the companion which perturbs the galaxy may determine the angular rate of the bar. Simulations of interaction-triggered bar formation (e.g., see Noguchi 1987; Salo 1991) indicate that bar pattern speeds are mostly dependent on the rotation curve and mass distribution of the galaxy. However, if a galaxy already has a bar before an interaction, then the interaction can modify not only the bar strength but also the bar pattern speed (Gerin *et al.* 1990; Sundin *et al.* 1993).

We note that really self-consistent simulations could change our view of these ringed galaxies substantially [see, e.g., Elmegreen *et al.* (1992) for a self-consistent study of the effects of interactions on outer rings]. In self-consistent models, it is not possible to vary the pattern speed as done in this paper, since the final pattern speed is probably determined by the shape of the potential (see Combes & Elmegreen 1993). In particular, as noted by the referee, very fast or very slow pattern speed simulations might not be realistic. Even so, the test-particle approach is clearly successful in explaining much about the structure of early type barred galaxies. It gives a good description of what occurs when the gas mass is negligible, as it likely is for our sample galaxies, and when the bar pattern speed is fixed in time.

The emphasis on early type galaxies is noteworthy because it is mostly among these galaxies where we find outer rings, especially the R_1' and R_2' subcategories. Combes & Elmegreen (1993) have shown that the bars of early and late type galaxies are fundamentally different in the sense that the former have high pattern speeds placing CR well within the disk, while the latter have low pattern speeds placing CR far outside the main structure. The high central concentration in early type galaxies nevertheless could explain why so many have nuclear rings. The pattern speeds, though high, still can allow an ILR for these galaxies. The predictions of Combes & Elmegreen (1993) are not inconsistent with much of our sample, but nevertheless do not yet readily explain cases like ESO 509−98.

Finally, we note that exceptions to what we have discussed here do exist. Our present models do not readily explain a *misaligned* bar/inner ring galaxy such as ESO 565−11 (see Fig. 11 in Buta & Crocker 1991, and Purcell *et al.* 1993), ringed barred spirals with flocculent outer spiral structure such as IC 5240 (Buta 1994; but see Combes & Elmegreen 1993), and various unusual bar morphologies such as are seen in ESO 509−98, NGC 7020 (Buta 1990b), and NGC 7098. There is thus much more to be learned about ringed galaxies than we have addressed with our simulations, and that will be covered in future papers.

We thank an anonymous referee for many helpful criticisms of the initial version of this paper. This work was supported by the Finnish Academy of Sciences (G.B.) and Grant Nos. NSF EPSCoR RII8996152 and AST 9014137. G.B. expresses appreciation for sabbatical support from the Space Telescope Science Institute.

REFERENCES

Buta, R. 1986a, ApJS, 61, 609
Buta, R. 1986b, ApJS, 61, 631
Buta, R. 1989, in The World of Galaxies, edited by H. Corwin and L. Bottinelli (Springer, New York), p. 29
Buta, R. 1990a, Annals New York Acad. Sci., 596, 58
Buta, R. 1990b, ApJ, 356, 87
Buta, R. 1991a, in Dynamics of Galaxies and Their Molecular Cloud Distributions, IAU Symposium No. 146, edited by F. Combes and F. Casoli (Kluwer, Dordrecht), p. 251
Buta, R. 1991b, ApJ, 370, 130
Buta, R. 1993, PASP, 105, 654
Buta, R. 1994, Proceedings of Ninth Florida Workshop on Nonlinear Astronomy, edited by S. T. Gottesman, H. Kandrup, J. Ipser, and G. Contopoulos (to be published)
Buta, R., & Crocker, D. A. 1991, AJ, 102, 1715
Buta, R., & Crocker, D. A. 1993, AJ, 105, 1344
Byrd, G. G., & Valtonen, M. 1987 AJ, 93, 811
Canzian, B. 1993, PASP, 105, 661
Combes, F., & Elmegreen, B. G. 1993, A&A, 271, 391
Combes, F., & Gerin, M. 1985, A&A, 150, 327
Combes, F., & Sanders, R. H. 1981, A&A, 96, 164
Contopoulos, G., & Grosbol, P. 1989, ARA&A, 1, 261
Crocker, D. A., & Buta, R. 1993, BAAS, 25, 1416
de Vaucouleurs, G. 1959, Handbuch der Physik, 53, 275
de Vaucouleurs, G. 1975, ApJS, 29, 193
Elmegreen, B. G., & Elmegreen, D. M. 1990, ApJ, 355, 52
Elmegreen, D. M., Elmegreen, B. G., & Bellin, A. D. 1990, ApJ, 364, 415
Elmegreen, D. M., Elmegreen, B. G., Combes, F., & Bellin, A. D. 1992, A&A, 257, 17
Friedli, D., & Martinet, L. 1993, A&A, 277, 27
Garcia-Burillo, S., Combes, F., & Gerin, M. 1993, A&A, 274, 148
Gerin, M., Combes, F., & Athanassoula, E. 1990, A&A, 230, 37
Jarvis, B., Dubath, P., Martinet, L., & Bacon, R. 1988, A&AS, 74, 513
Kalnajs, A. 1992, in Dynamics of Disk Galaxies, edited by B. Sundelius (Goteborg University, Sweden), p. 323
Kenney, J., Carlstrom, J. E., & Young, J. D. 1993, ApJ, 418, 687
Kent, S. M. 1987, AJ, 93, 1062
Kent, S. M., & Glaudell, G. 1989, AJ, 98, 1588
Mihalas, D., & Binney, J. 1981, Galactic Astronomy (Freeman, New York)
Noguchi, M. 1987, MNRAS, 228, 635
Pfenniger, D., & Norman, C. A. 1990, ApJ, 363, 391
Purcell, G. B., Buta, R., & Crocker, D. A. 1993, BAAS, 25, 1413
Salo, H. 1991, A&A, 243, 118
Schwarz, M. P. 1979, PhD. thesis, Australian National University
Schwarz, M. P. 1981, ApJ, 247, 77
Schwarz, M. P. 1984, MNRAS, 209, 93
Schwarz, M. P. 1985, MNRAS, 212, 677
Sellwood, J. 1981, A&A, 99, 362
Sellwood, J. A., & Sparke, L. S. 1988, MNRAS, 231, 25P
Sellwood, J. A., & Wilkinson, A. 1993, Rep. Prog. Phys., 56, 173
Shaw, M., Combes, F., Axon, D. J., & Wright, G. S. 1993, A&A, 273, 31
Solomon, P. M. and Sanders, D. B. 1986, Protostars and Planets II, edited by D. C. Black and M. S. Matthews (University of Arizona Press, Tucson), p. 59
Sparke, L. S., & Sellwood, J. A. 1987, MNRAS, 225, 653
Sundin, M., Donner, K. J., & Sundelius, B. 1993, A&A, 280, 105
Tremaine, S., & Weinberg, M. D. 1985, ApJ, 282, L5
Verschuur, G. L. 1993, AJ, 106, 2580